DOI 10.1007/s10553-024-01699-6
Chemistry and Technology of Fuels and Oils, Vol. 60, No.2, May, 2024 (Russian Original No.2, March– April, 2024)

INNOVATIVE TECHNOLOGIES OF OIL AND GAS

STUDY ON THE DIVISION OF REMAINING RECOVERABLE RESERVES ABUNDANCE IN SPECIFIC RESERVOIRS

Le Qu[1,2,3] ✉, Xiaolei Zheng[1,2], Weigang Zhang[4], Jianping Liu[5], Yanan Zhu[6], Zhenzhen Nian[1,3], Kexiang Ning[1,3], Zhe Zhang[1,3]

The Yanchang group Chang 6 reservoir in the Tiebiancheng area, after decades of exploitation, exhibits localized zones of relatively high permeability but is predominantly characterized as an extra-low permeability oil reservoir with minimal natural productivity. The reservoir's strong heterogeneity poses challenges in achieving production targets, resulting in significant variations in well yields. Therefore, a scientific division of potential zones within the blocks, targeted exploitation strategies are necessary. This study classifies the recoverable reserves abundance of the Chang 6 reservoir in the Tiebiancheng area into four distinct types, based on the analysis of two oilfield indicators: material potential field and flow state field. These types are categorized as follows: high velocity and high abundance (Type I), low velocity and high abundance (Type II), high velocity and low abundance (Type III), and low velocity and low abundance (Type IV). Moreover, tailored exploitation strategies are proposed, considering the characteristics of different favorable target zones. A computational simulation of regional oil production, with zoning exploitation strategies taken into account, indicates an anticipated cumulative oil production of 1463·10⁴ m³ by 2027, whereas the cumulative oil production of the control group is projected to reach 1387·10⁴ m³, resulting in a notable difference of 76·10⁴ m³, signifying a considerable improvement in the recovery rate.

Keywords: Chang 6 reservoir, remaining recoverable reserves, abundance zoning, exploitation strategy.

1. Introduction

The Jiyuan Oilfield, located in the central western part of the Ordos Basin, is a significant tight oilfield. The Tiebiancheng area, situated at the southeast edge of the oilfield, has emerged as a key exploration block of the Changqing Oilfield in recent years [1-7]. With advancements in exploration techniques and a deeper understanding of the oilfield, new discoveries have been made in the Chang 6 reservoir group within the Tiebiancheng area, leading to a breakthrough in the yield of the Chang 6_1 reservoir group. However, these developments have also brought forth a set of new challenges during exploitation, including complex oil and water distribution, rapid increase in water cut [8, 9]. Consequently, this study aims to address these issues by dividing the

[1] Xi'an Shiyou University, Xi'an, Shaanxi, China; [2] Shaanxi Key Laboratory of Petroleum Accumulation Geology, Xi'an, Shaanxi, China; [3] Xi'an Key Laboratory of Tight oil (Shale oil) Development (Xi'an Shiyou University), Xi'an, Shaanxi, China; [4] No.8 Oil Recovery Plant of PetroChina Changqing Oilfield Company, Xi'an, Shaanxi, China; [5] Exploration Department of PetroChina Changqing Oilfield Company, Xi'an, Shaanxi, China; [6] No.5 Oil Recovery Plant of PetroChina Changqing Oilfield Company, Xi'an, Shaanxi, China. *Corresponding author: Le Qu ✉. E-mail: qiaozhouqcfff168@163.com.* Translated from *Khimiya i Tekhnologiya Topliv i Masel*, No. 2, pp. 167–172, March– April, 2024.

abundance zoning of remaining recoverable reserves in the Tiebiancheng area's Yanchang Group Chang 6 reservoir based on two reservoir flow field characteristics: material potential field and flow status field. Corresponding development strategies for the later stages are formulated with the objective of enhancing the recovery rate of the remaining reservoirs in the study area.

2. Physical properties of Long 6 within Tiebian City Region

Porosity and permeability features. In general, numerical characterization of reservoir properties is achieved through the assessment of permeability and porosity. To investigate these properties, quantitative or semiquantitative methods are utilized, which aids in the evaluation of reservoir characteristics. The study area exhibits a porosity ranging from 6% to 12%, with an average value of 9.8%. Conversely, the permeability is primarily below 0.8 mD, with an average value of 0.18 mD. With a very low to ultra-low permeability, the reservoir is characterized by these values. It is worth mentioning that there are substantial discrepancies in the frequency distribution of porosity and permeability across various layers. These variations suggest a noteworthy alteration in physical properties from Long 6_1^1 to Long 6_3^2.

Porosity-permeability relationship. Statistical analysis of the petrophysical data from core samples in the study area reveals that permeability increases with the increase in porosity values. This relationship indicates that the storage and permeability capacity of the sandstone is still largely dependent on thematrix pores and throats of the sandstone to a certain extent. The low values of porosity and permeability reflect the fine nature of the throats and pores in the study area's reservoirs. Nonetheless, micro-fractures play a certain role in enhancing the permeability of the reservoir (**Figure 1**).

Zoning of remaining recoverable potential based on aquifer subdivision. The evaluation of the abundance of remaining recoverable reserves must be a comprehensive analysis based on multiple factors, including the porosity of the strata, thickness, and remaining oil saturation, amongst others, to fully assess the actual exploitation potential of the reservoir [10, 11]. However, In the study area, the physical properties of the reservoir are relatively poor, impacting the accumulation of oil and gas. Consequently, a distinct boundary exists between the bottom water and the reservoir, leading to lower potential for later-stage development. Therefore, the initial step involves determining the water-flooded areas within the reservoir to delineate the potential and water-flooded zones. Subsequent divisions can be made based on these potential zones.

Determination of aquifer zones. In this study, new geological research findings and production data of the Chang 6 reservoir group are utilized to analyze the aquifer zones [12, 13]. By employing the principle of flow material balance, the pressure drop(ΔP) and cumulative liquid production of the reservoir can be graphically represented in rectangular coordinates, facilitating the accurate determination of aquifer zones within the study area. The pressure drops and cumulative liquid production ($N_pB_o + W_pB_w - W_{inj}B_w$) of the Chang 6 reservoir group exhibit four distinct forms, as illustrated in **Figure 2**.

Curve *1* primarily indicates the stable characteristics of the aquifer under rigid water drive. In this case, the expansion of the aquifer water effectively compensates for the depletion caused by oil production, resulting in no pressure drop throughout the reservoir during production. Curve *2* mainly signifies pure elastic drive of oil, typically observed in regions with secondary

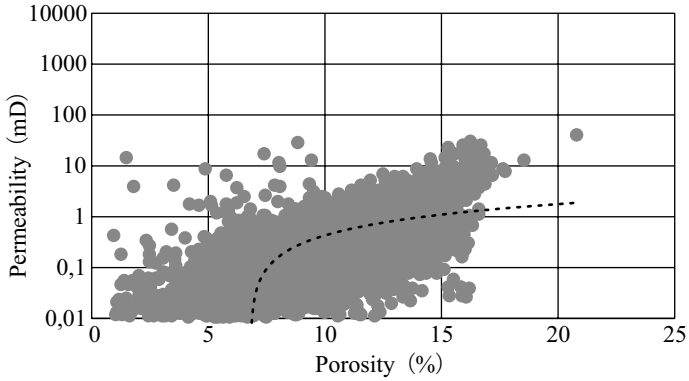

Fig. 1. Relationship between pores and permeability of Layer 6

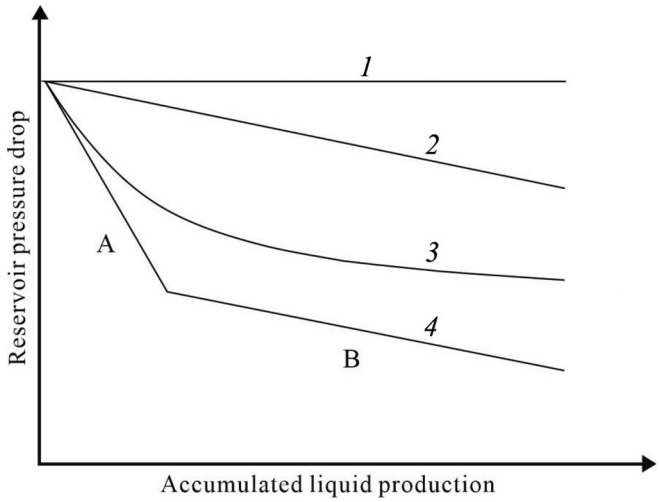

Fig. 2. Four typical pressure drop curves of reservoirs

fracture development. The reservoir exhibits a relatively closed isochore. The aquifer is poorly developed, and artificial water injection can directly replace oil production after rapid blowdown. Curve *3* primarily indicates elastic water drive, which occurs through the interaction of water encroachment and the elastic expansion of oil. The specific amount of water encroachment and the size of the aquifer can be determined through material balance and the Fetkovich aquifer models.

Following the principle of material balance, the material balance equation for an oil reservoir is as equation:

$$N_P B_o + W_P B_w - W_{inj} B_w = N B_{oi} c_{eff} \Delta P + W_e, \tag{1}$$

where, N_p represents the cumulative oil production; B_o denotes the oil formation volume factor; W_p signifies the cumulative water production; W_{inj} represents the water injection amount; B_w stands for the water formation volume factor; c_{eff} denotes the comprehensive compression coefficient of the reservoir; B_{oi} refers to the current oil formation volume factor; N represents the geological reserves; W_e represents the amount of water invasion; ΔP denotes the pressure drop in the reservoir.

This study employs the Fetkovich method to calculate the water parameters and the amount of water invasion. The specific calculation equation is given by equation:

$$W_e = \frac{W_{ei}}{P_i}\left(P_i - P\right)\left(1 - \mathrm{e}^{-\frac{J_e P_i}{W_{ei}}}\right),\ W_{ei} = V_w C_t P_i, \tag{2}$$

where, V_w represents the size of the water body; W_{ei} denotes the cumulative water invasion amount; C_t expresses the compression coefficient of water; P_i represents the pressure at any time, and J_e represents the water invasion index.

By combining Equations (1) and (2), material balance analysis can be conducted using the following calculation equation, as shown in equation:

$$\frac{N_P B_o + W_P B_w - W_{inj} B_w}{\Delta P} = \frac{W_{ej}}{P_i}\left(1 - \mathrm{e}^{-\frac{J_e P_i}{W_{ej}}}\right) + B_{oi} c_{eff} \Delta P,$$

$$\text{Let, } X = W_{ej}\left(1 - \mathrm{e}^{-\frac{J_e P_i}{W_{ej}}}\right),\ Y = \frac{N_P B_o + W_P B_w - W_{inj} B_w}{\Delta P}. \tag{3}$$

Subsequently, the result is given by equation:

$$Y = kX + N B_{oi} c_{eff}. \tag{4}$$

By combining Equations (2) and (4) and utilizing the classical genetic algorithm, it is possible to calculate the size of the water body and the amount of invasion.

Curve *4* represents the elastic water pressure drive, indicating the occurrence of water invasion after the release of elastic energy. During this stage, the region experiences an increasing enrichment of oil and gas, accompanied by the development of a corresponding bottom water layer at a certain scale. As the dissolution depth continues to increase, effective communication with the water body is established [15]. The pressure drop rate gradually extends throughout the water body, leading to a decrease in the energy of the oil-water system. The water invasion rate becomes more prominent than the pressure drop, exhibiting typical steady-state characteristics and an overall inflection point-linear morphology [16].

Segment A of Curve *4* effectively drives the pure elasticity of oil within the reservoir. The specific material balance equation for the reservoir in this stage is given by equation:

$$N_P B_o + W_P B_w - W_{inj} B_w = N B_{oi} c_{eff} \Delta P, \tag{5}$$

The straight-line segment B represents the mixed driving stage after water invasion. Given the water invasion presents quasi-stable characteristics, the calculation equation for the amount of water invasion is given by equation (6):

$$W_e B_w = V_w B_w C_w \Delta P_2, \tag{6}$$

Due to the unique characteristics of this stage in the material balance process, the calculation is given by equation:

$$N_P B_o + W_P B_w - W_{inj} B_w = N B_{oi} c_{eff} \left(\Delta P_1 + \Delta P_2\right) + V_w B_w C_w \Delta P_2, \tag{7}$$

where, ΔP_1 represents the pressure drop in the elastic stage; ΔP_2 represents the pressure drop in the water invasion stage, both of which are known quantities.

By combining Equations (5), (6), and (7) for calculation, the calculation results of the water body size and water invasion amount can be obtained.

Analyzing the water invasion characteristics of the Chang 6 oil formation in the Tiebiancheng region prior to the occurrence of water flooding, we begin by classifying the aforementioned concepts. Verification outcomes can be acquired by performing the computation of water body energy and water invasion amount, followed by their integration with unit numerical models, verification results can be obtained. The results indicate that curves *1*, *2* and *3* all correspond to unsteady-state water invasion. Curve *4* represents quasi-steady water invasion. Additionally, the unit water body scale is determined to be $44265 \cdot 10^4\ m^3$, with a water body multiple ranging from 26.8 to 27.8 times, classifying it as a medium-sized water body. Considering the actual conditions of the water-flooded area, a water saturation of 0.9 or above is set to determine the water body area [17]. Based on the calculations from Curve *4*, the water content within this area is determined to be 0.93, confirming its classification as a water body area.

Potential zoning measures. In this study, the potential zones of the Chang 6 oil reservoir in the research area are identified, taking the encryption new well regulation and control strategy as an example. The low potential zone requires optimization of injection and production parameters to meet mining requirements, while the high potential zone represents the main mining area in the later stages.

Based on economic factors, the economic limit cumulative oil production of a single well is calculated based on the breakeven point [18]. The specific equation is formulated as equation:

$$N_{pe} = \frac{I_d + I_b + C_0 \dfrac{\left(1+i\right)^T - 1}{i}}{\omega\left(P_0 - R_T - R_0\right)}, \tag{8}$$

where, I_d, I_b, and C_0 represent the drilling investment, ground construction investment, and initial single well operating cost, respectively; N_{pe} represents the economic limit cumulative oil production of a single well; P_0, R_0, and R_T represent the current crude oil price, the cost that can vary per ton of oil, and the tax per ton of oil, respectively; ω represents the commodity rate of crude oil; T represents the investment payback period.

According to the maximum recoverable reserves obtained in Equation (1), the abundance of the economic limit remaining reserves per well can be calculated as equation:

$$I_{pe} = \frac{N_{pe}}{A}, \tag{9}$$

where, A represents the control area of a single well; I_{pe} represents the abundance of the economic limit remaining reserves per well.

Following the above results, the actual remaining reserves abundance in the reservoir can be obtained, and the specific equation satisfies as equation:

$$I_0 = 100h\varphi\left(S_0 - \overline{S}_{or}\right)\rho_0 / B_0, \tag{10}$$

where, h represents thickness; S_0 and B_0 represent saturation and volume factor, respectively; where φ denotes the height; ρ_0 represents original oil density; $\overline{S}_{or}$ represents the remaining oil saturation after the end of mining, which can be calculated based on related empirical reports, and the specific equation is formulated as equation:

$$\overline{S}_{or} = -0.013l \ln \Re + 0.1946, \tag{11}$$

where, $\Re$ represents the permeability of the formation.

Based on Equation (10), the calculation of Equation (11) can be completed to obtain the modified equation:

$$I_0 = 100h\varphi\left(S_0 + 0.131\ln \Re - 0.1946\right)\rho_0 / B_0. \tag{12}$$

If the I_0 result is greater than I_{pe}, the reservoir area can serve as an adjustment and control area. If it is lower than I_{pe}, the reservoir area can serve as an injection and production adjustment and control area.

According to the above equation (1), it can be determined that the limit cumulative oil production of a single well in the target area is $5.6 \cdot 10^4$ t, and the control area is 0.282 km^2. According to Equation (2), the abundance of the economic limit remaining reserves per well is 0.196 t/km^2. Based on this, the division of areas with recoverable reserves abundance is completed, as shown in **Figure 3**.

Based on the analysis depicted in Figure 3, it is observed that the delta distributary channel sand body of the Chang 6_1 reservoir exhibits significant development, particularly the small layer of Chang 6_1^2. The southern part of the study area displays a high sand-land ratio, indicating the presence of large-scale single sand bodies with considerable potential. Evaluation based on predefined criteria reveals that the favorable targets within the Chang 6_1 reservoir are predominantly concentrated in the southern

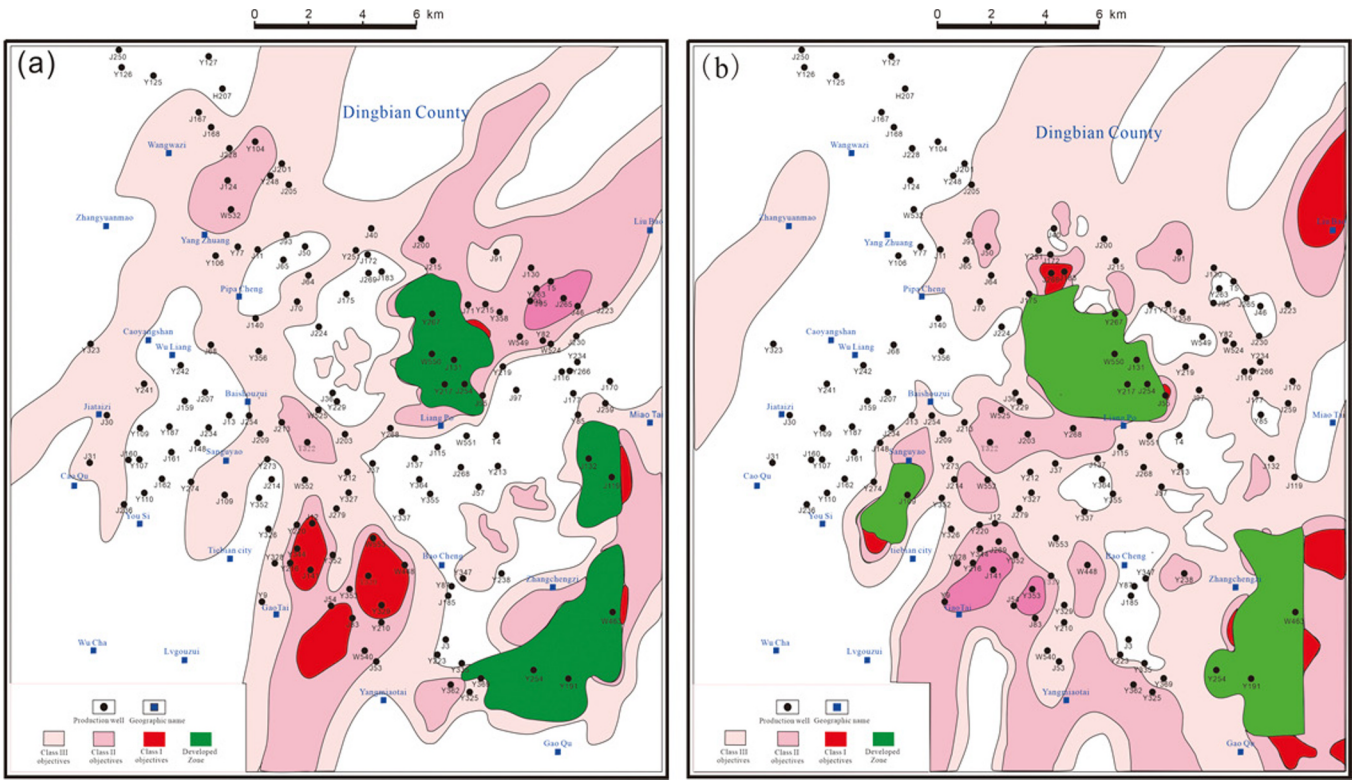

Fig. 3. Abundance partition distribution map of potential production areas for Chang6_1^1 and Chang6_1^2

region. The Class I production targets are primarily found in the J12, J83, W553, and J269 well areas, covering an area of 10.2 km^2 and possessing a reserve scale of $2.9 \cdot 10^6$ t. On the other hand, the Class II production zones encompass the J95, J141, and Y353 well areas, spanning an area of 7 km^2 and featuring a reserve scale of $1.95 \cdot 10^6$t. In total, these production zones exhibit a combined production potential of $4.85 \cdot 10^6$t.

3. Delineation of potential areas based on effective seepage velocity

The delineation of potential areas based on remaining reserves abundance can dynamically grasp the distribution of potential development zones, which is primarily determined through development schedule, reservoir properties, and methods. High abundance can serve as the main development region. For areas with relatively poor well pattern and low control degree, targeted regulation strategies must be adopted, thus necessitating an understanding of seepage velocity [19]. This insight can help researchers more objectively grasp the actual flow status of reservoir fluids and develop flow field control strategies for the improved recovery of remaining reservoirs.

Under economic factors, the seepage velocity corresponding to the economic limit liquid production of a single well is adopted to complete the delineation of high flow velocity and low flow velocity regions which satisfies as equation [20, 21]:

$$Q_L = \frac{C_G \cdot 10^4 / 365}{(1 - f_w)(P_O - R_T) - C_V}, \tag{13}$$

where, C_G represents the annual fixed cost per well; Q_L represents the economic limit liquid production of a new well; C_V represents the variable cost per ton of liquid; f_w represents water cut.

The following liquid flow velocity can be obtained by combining the actual reservoir thickness and well spacing, which is given by equation:

$$v_{tc} = \frac{Q_L}{B \cdot h}, \tag{14}$$

where, B represents the reservoir well spacing.

The limit liquid production of a single well in this reservoir is calculated to be 38t/d based on the economic evaluation results. The liquid flow velocities corresponding to the thickness, water cut, and economics of different networks can be obtained. The average flow velocity is $1.13 \cdot 10^{-6}$ m/s, serving as the standard for low flow velocity and high flow velocity. Based on Darcy's law and reservoir simulation results, the seepage velocity in the x-direction can be expressed as equations:

$$v_{ox}(i) = \begin{cases} -\dfrac{KK_{ro}(i)}{\mu_o(i)} \dfrac{P_o(i) - P_o(i+1)}{\Delta x}, & i = 1, 2, \cdots, n\text{-}1 \\ v_{ox}(i-1), & i = n \end{cases} \tag{15}$$

$$v_{wx}(i) = \begin{cases} -\dfrac{KK_{rw}(i)}{\mu_w(i)} \dfrac{P_w(i) - P_w(i+1)}{\Delta x}, & i = 1,\ 2, \cdots, n-1 \\ v_{wx}(i-1), & i = n \end{cases} \tag{16}$$

where, K represents permeability; P_o and P_w represent oil phase and water phase pressures, respectively; K_{ro}, K_{rw} represent oil phase and water phase permeabilities, respectively; μ_o, μ_w represent oil phase and water phase viscosities, respectively.

Based on this, Equations (8) and (9) can be used to obtain the seepage velocity in the x-direction as equation:

$$v_x(i) = v_{ox}(i) + v_{wx}(i). \tag{17}$$

Similarly, the seepage velocity in the y-direction can be obtained as equation:

$$v_y(i) = v_{oy}(i) + v_{wy}(i). \tag{18}$$

Vectorially adding the above two equations gives the grid fluid flow velocity as equation:

$$v_t(i) = \sqrt{v_x(i)^2 + v_y(i)^2}. \tag{19}$$

Based on this result and the above standard, if v_t is greater than v_{tc}, it indicates that the seepage velocity of the fluid in the grid exceeds the liquid flow velocity and belongs to the high flow velocity region. If v_t is less than v_{tc}, it indicates that the seepage velocity of the fluid in the grid is lower than the liquid flow velocity and belongs to the low flow velocity region.

4. Reservoir abundance zoning and development strategies

Comprehensive zoning of reservoir abundance. By combining material potential and flow conditions, four different abundance zoning standards are formulated, including low flow speed and low abundance, low flow speed and high abundance, high flow speed and low abundance, as well as high flow speed and high abundance. Specifically, as depicted in **Table 1**, the low speed and high abundance area represents the area where the remaining oil reservoirs can be exploited, thus becoming an important area for well network densification and injection optimization in the later period of oilfield development.

Development strategies. In general, the reservoirs in Tiebiancheng area can fall into several zones based on the integrated abundance zoning standards of material potential and flow conditions. The grid classification results of different zones can be obtained through numerical simulation. Combined with the characteristics of different types of areas, overall planning can be made, actual areas can be counted, and development strategies can be provided for later development. The relevant details are listed in **Table 2**.

Based on the actual situation of the oilfield, the evaluation units are formed with the Chang6_3^2, Chang6_3^1, Chang6_2^2, Chang6_2^1, Chang6_1^2, Chang6_1^1 and other six sublayers, and a total of 13 favorable target areas are evaluated in the six sublayers, as illustrated in **Table 3**. Specifically, there are four type I favorable target areas, six type II favorable target areas, and three type III favorable target areas. Type I takes up an area of 10.2 km^2, with a reserve scale of $2.9 \cdot 10^6$ t; the area of type II is 13.7 km^2, with a reserve scale of $3.8 \cdot 10^6$ t; the area of type III is 7.1 km^2, with a reserve scale of $1.5 \cdot 10^6$ t. The total confirmed production target is $8.2 \cdot 10^6$ t.

The actual abundance of type I areas must be greater than the economic limit abundance in accordance with the above integrated zoning results and development strategies, which can serve as key development areas. Specifically, type II areas show low speed characteristics, and there is a lack of completion of the well network, which can serve as potential development areas after future well network densification and regulation. The type I target areas in this study area have a perfect well network that can conform to the requirements of current development, and no adjustments should be made [21]. Comprehensively considering the current well network situation, nine infill wells should be arranged and deployed in type II areas to ensure future development needs. Furthermore, the zoning results of potential areas reveal that appropriate injection optimization strategies must be carried out for wells in type III areas, so as to optimize the amount of injected water and produced fluid.

Table 1. Comprehensive abundance zoning standards based on material potential and flow conditions

Index	High Flow Speed and High Abundance (Type I)	Low Flow Speed and High Abundance (Type II)	High Flow Speed and Low Abundance (Type III)	Low Flow Speed and Low Abundance (Type IV)
Remaining Recoverable Reserves Abundance (10^4t/km^{-2})	>19.6	>19.6	<19.6	<19.6
Liquid Flow Velocity (10^{-6}m/s^{-1})	>1.13	<1.13	>1.13	<1.13

Table 2. Area statistics and strategies under abundance zoning standards

Zone	Proportion of Area (%)			Strategies
	Zone 1	Zone 2	Zone 3	
High Speed and High Abundance (Type I)	8.7	3.3	1.6	Has good mobility, can serve as a key development area
Low Speed and High Abundance (Type II)	9.6	6.7	1.5	The potential area needs to densify and regulate the well network
High Speed and Low Abundance (Type III)	33.4	7.2	2.0	Inhibit water injection
Low Speed and Low Abundance (Type IV)	2.1	1.9	1.6	Not suitable for new well densification, appropriate injection and production optimization is needed

Table 3. Statistics of favorable areas in Chang6 of Tiebiancheng area

Tier Positions	Well area	Sand layer (m)	Oil layer (m)	Resistivity (m)	Velocity of sound (μs/m)	Apparent porosity (%)	Apparent permeability (mD)	Contains saturation (%)	Favorable area (km^2)	Reserve size (tons)	Type of favorable area
$Chang6_1$	J95	10.9	6.8	14	235	11.7	0.61	31	2.2	60	Class II
	J12	12.3	7.4	16	239	13.1	0.74	37	2.4	70	Class I
	J83	11.3	6.1	21	221	10.4	0.47	36	3.1	80	Class I
	W553	12.5	6.8	15	226	11.8	0.51	39	2.5	75	Class I
	J269	10.8	6.2	18	231	10.2	0.61	35	2.2	65	Class I
	J141	11.3	8.1	26	237	12.2	0.34	41	3.1	85	Class II
	Y353	10.3	6.3	17	225	11.4	0.27	35	1.7	50	Class II
$Long\ 6_2$	Y16	11.7	6.3	23	230	11.9	0.31	31	2.1	45	Class III
	J124	10.2	6.5	27	237	11.5	0.59	40	2.3	65	Class II
	J230	10.4	6.1	32	229	10.0	0.25	35	3.2	60	Class III
$Long\ 6_3$	J177	9.3	6.1	41	229	9.5	0.37	41	1.9	55	Class II
	Y335	12.1	6.7	42	231	10.7	0.37	42	2.5	65	Class II
	J83	11.2	7.1	41	224	10.3	0.21	36	1.8	45	Class III
Total		11.1	6.7	26	230	11.1	0.43	37	31	820	–

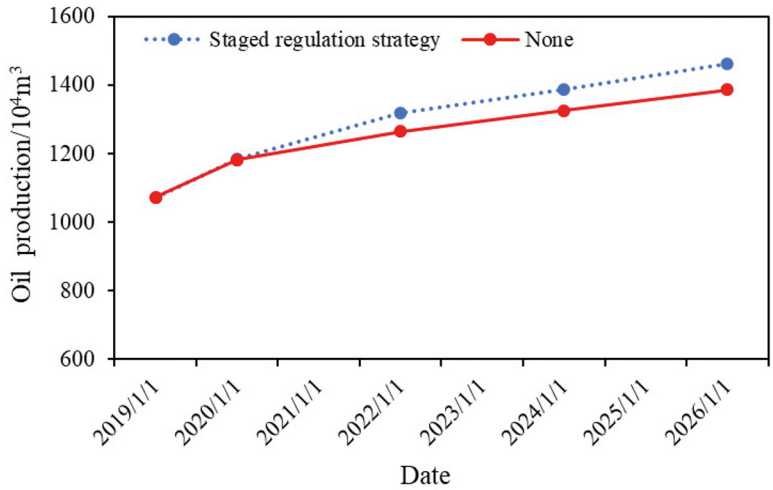

Fig. 4. Cumulative oil production forecast curve

Effect prediction of reservoir abundance zoning. Based on the development arrangements and deployments described above, an evaluation of oil production in the study area is conducted using numerical simulation. A control model is established to compare the results in the absence of any intervention measures. The findings, as depicted in **Figure 4**, reveal that the initial cumulative oil production is approximately $1073 \cdot 10^4\ m^3$. After 7 years of development, the water cut within the block is projected to rise to 90%. However, with the implementation of the proposed development strategy based on zoning, it is anticipated that by 2027, the cumulative oil production will reach $1463 \cdot 10^4\ m^3$, whereas the control group's cumulative oil production is estimated to reach $1387 \cdot 10^4\ m^3$. The difference between the two amounts to $76 \cdot 10^4\ m^3$, providing substantial evidence that this scheme significantly enhances the recovery rate of the oil reservoirs.

5. Conclusions

This study focuses on the remaining recoverable reserves abundance of reservoirs in the Tiebiancheng area as the basis for formulating development strategies. Economic factors are comprehensively considered, and the economic limit residual per well is utilized as a criterion for dividing potential regions. Additionally, numerical simulation is employed to calculate the seepage

velocity of fluids within the Tiebiancheng reservoirs, using the cumulative daily production corresponding to the economic limit as a benchmark for evaluating the seepage velocity of different regions.

By integrating material potential and flow conditions, a comprehensive abundance zoning standard is established, resulting in the classification of reservoirs into four levels: high speed and high abundance (Type I), low speed and high abundance (Type II), high speed and low abundance (Type III), and low speed and low abundance (Type IV). Thirteen sweet spots are identified in the I, II, and III categories, covering a total area of 31km^2 and possessing a combined development potential of $8.2 \cdot 10^6$ t. Corresponding development strategies are proposed based on the different target types.

Using numerical simulation with a control group as a reference, the future production impact of the formulated zoning and control strategy is predicted for the oilfield. Under the zoning development strategy, it is anticipated that by 2027, the cumulative oil production will reach $1463 \cdot 10^4$ m^3, while the cumulative oil production of the reference group will be $1387 \cdot 10^4$ m^3. These results demonstrate that the proposed scheme is favorable for increasing the recovery rate.

Acknowledgements

The authors appreciate the financial support of the National Natural Science Foundation of China (No.52004223), the Technology Innovation Leading Program of Shaanxi (No.2022PT-08), and the Project of Youth Innovation Team of Shaanxi Universities (22JP063).

REFERENCES

1. Yao, X. T., Su, X. K., Zheng, X., et al. 3D physical simulation experiments of development effects after well pattern adjustment in extra-high water cut reservoirs. *Petroleum Geology and Recovery Efficiency,* 2023, *30*(01), 139-145.

2. Fan, T. E., Du, X., Fan, P. J., et al. Fault-Landform Double Controlled Archean Buried-Hill Reservoir Integrated Prediction for BZ26-6 Oil Field, Bohai Bay. *Earth Science,* 2023, *48*(2), 429-438.

3. Yin, S., Mei, H., Xu, X. Experimental Study on Dynamic and Static Rock Mechanical Properties of Tight Sandstone Gas Reservoir. *Chem Technol Fuels Oils*, 2023, 59, 561-568.

4. Chai, R. K., Liu, Y. T., He, Y. T. et al. Low-salinity waterflooding laws in the tight sandstone oil reservoirs of Yanchang Formation in Ordos Basin. *Daqing Petroleum Geology and Development,* 2022, *41*(2), 67-74.

5. Li, M., Liao, J., Wang, S., et al. Imbibition characteristics and influencing factors of reservoirs with ultra-low permeability of Ordos Basin:a case study of third memThassic Yanchang: in Weibei Oil Field. *Petroleum Geology Experiment*, 2022, *44*(6), 971-980.

6. Zhao, D. L., Bai, Y. B., Zhang, H. Characteristics and Reservoir-Forming Model of Yan 9 Reservoir in Jingbian Oilfield, Ordos Basin. *Xinjiang Geology,* 2022, *40*(3), 388-393.

7. Liu, C. C., Yang, Y. X., Fang, T. Y., et al. Evaluation method of highquality shale oil reservoir in Ordos Basin. *Well Logging Technology,* 2023, *34*(03), 49-54+62.

8. Zhang, X. L., Tang, Y., Li, Z.Y., et al. Hydrocarbon Accumul-ation Patterns of Chang 8 Low-Charging Oil Reservoirs in Southwestern Margin of Ordos Basin: Taking Huanxi-Pengyang Area as an Example. *Journal of Xi'an Shiyou University,* 2023, *38*(1), 31-44.

9. Zhang, X. M., Huang, M., Li, K., et al. Reservoir forming model and main controlling factors of Jurassic reservoir in Tiebiancheng area. *Application of Petrochemical Technology,* 2022, *41*(7), 81-85.

10. Ji, B.Y., Xu, T., Gao, X.J., et al. Production evolution patterns and development stage division of waterflooding oilfields. *Petroleum Exploration and Development, 2023*, 50(2), 433-441.

11. Cui, C. Z., Li, S., Yang, Y., et al. Planar zoning regulation and control method of reservoir at ultra-high water cut stage. *Petroleum Exploration and Development,* 2018, *39*(10), 1155-1161.

12. Naderi, M., Khamehchi, E. Well placement optimization using metaheuristic bat algorithm. *Journal of Petroleum Science & Engineering,* 2016, *150*(13), 348-354.

13. Lyons, J., Nasrabadi, H. Well placement optimization under time-dependent uncertainty using an ensemble Kalman filter and a genetic algorithm. *Journal of Petroleum Science & Engineering,* 2013, *109*(9), 70-79.

14. Jia, H.Z., Li, B.Y., Lyu, Z., et al. Experimental study on the interaction between CO_2 and Jimsar reservoir rocks. *Chemical Engineering of Oil & Gas*, 2021, 50(1), 76-80.

15. Li, J.X., Liu, Y., Wu, D., et al. The Synergistic Effects of Alkaline, Surfactant, and Polymer on the Emulsification and Destabilization of Oil-in-water Crude Oil Emulsion Produced by Alkaline-surfactant-polymer Flooding. *Petroleum Science & Technology,* 2013, *31*(4), 399-407.

16. Supee, A., Idris, A. K. Effects of Surfactant-Polymer Formulation and Salinities Variation Towards Oil Recovery. *Arabian Journal for Science and Engineering,* 2014, *39*(5), 4251-4260.

17. Wang, G. F., Song, L. Z., Wei, Z. L., et al. A Laboratory Study of Polymer and Surfactant Binary Combination Flooding in Reservoirs with Low to Medium Permeability. *Advanced Materials Research,* 2013, 718-720.

18. Guan, X.W., Meng, Q., Wang, B.B., et al. Description of Formations Fault Activity Characteristics and Genesis Mechanism Using of Paleogeomorphic Restoration Techniques. *Chem Technol Fuels Oils*, 2023, 59, 647-660.

19. Lyu, X., Zhu, G., Liu, Z. Well-controlled dynamic hydrocarbon reserves calculation of fracture–cavity karst carbonate reservoirs based on production data analysis. *Journal of Petroleum Exploration and Production Technology*, 2020,10, 2401-2410..

20. Ren, M. Y., Shi, Q., Xin, H. Z., et al. Characteristics of Remaining Oil Distribution in Conglomerate Reservoirs after Water Flooding and Technical Countermeasures. *Special Oil & Gas Reservoirs,* 2023, *30*(1), 147-153.

21. Dong, Y. W., Wang, R., Wang, S. Y., et al. Evaluation of Oil Displac-ement Effect and Microscopic Oil Displacement Mechanism of Viscoelastic Fluid with Low Interfacial Tension. *Science Technology and Engineering,* 2023, *23*(3),1017-1023.